Biocybernetics and Biomedical Engineering

Original Research Article

Extracting tumor in MR brain and breast image with Kapur's entropy based Cuckoo Search Optimization and morphological reconstruction filters

Check for updates

R. Sumathi [a,*], *M. Venkatesulu* [b], *Sridhar P. Arjunan* [c,d]

[a] *Department of Computer Science and Engineering, Kalasalingam Academy of Research and Education, Tamil Nadu, India*
[b] *Department of Information Technology, Kalasalingam Academy of Research and Education, Tamil Nadu, India*
[c] *Electronics and Instrumentation Engineering, SRM Institute of Science and Technology, Tamil Nadu, India*
[d] *Biosignals Lab, RMIT University, Melbourne, Australia*

ABSTRACT

Magnetic Resonance Imaging (MRI) scanners are used to determine the presence of tumors in human bodies. In clinical oncology, algorithms are heavily used to analyze and identify the tumor region in the slice images produced by the MRI scanners. This article presents an unique algorithm which is developed based on Kapur's Entropy-based Cuckoo Search Optimization and Morphological Reconstruction Filters. The former is used to locate and segment the boundary of tumors, while the later to remove unwanted pixels in the slice images. The proposed method yields 97% accuracy in the identification of the exact topographical location of tumor region. It requires less computational time (about 3 milli-seconds, on average) for processing. Thus the proposed method can help radiologists quickly detect the exact topographical location of tumor regions even when there are severe intensity variations and poor boundaries. The method fares well in terms also of other standard comparison metrics like entropy, eccentricity, Jaccard Index, Hausdorff distance, MSE, PSNR, precision, recall and accuracy, when compared to the existing methods including Fuzzy C Means clustering and PSO. Above all, the algorithm developed can detect the tumor regions in the MR images of both brain and breast. The method is validated using various types of MR images (T1, T2 for MRI brain, and T1 post contrast and post processed images for breast) available in the online datasets of BRATS, RIDER and Harvard.

© 2018 Nalecz Institute of Biocybernetics and Biomedical Engineering of the Polish Academy of Sciences. Published by Elsevier B.V. All rights reserved.

* Corresponding author at: Department of Computer Science and Engineering, Kalasalingam Academy of Research and Education, Tamil Nadu, India.
E-mail addresses: suchandika@gmail.com (R. Sumathi), venkatesulum2000@gmail.com (M. Venkatesulu), sridhararjun@gmail.com (S.P. Arjunan).

1.   Introduction

Medical image segmentation is about dividing an image into many homogeneous parts, which are used for analysis and synthesis of various real-time applications. It employs various methods such as threshold, clustering, compression, histogram, edge detection, region growing, split and merge, and neural networks techniques. Clustering is an important method applied in medical image processing. It is defined as the process of organizing the objects into various groups and share common characteristics among members of a group. Similarly, optimization is the process of modifying a system into features so as to work more efficiently within given constraints and to maximize the desired parameters and to minimize the undesired parameters that are involved as discussed in Yang et al. [1,2]. Cuckoo Search Optimization is used to optimize the objective function, and also choose the segmentation threshold for achieving the best segmentation result. It avoids exhaustive search and is useful in identifying the solutions for non-linear problems. It supports multi-objective optimization techniques.

Mathematical morphology is used in various images processing operations and has become the foundation of biomedical computing. Image segmentation is a vital component of image analysis, which partitions the whole image into disjoint regions based on potential features such as color, texture, and gray value as reported by Roushdy [3]. Pratheeba et al. [4] applied Cuckoo Search Optimization for classifying the healthy and pathological tissues in Magnetic Resonance Image (MRI) brain images. EliseeIlunga-Mbuyamba et al. [5] proposed an active contour model driven by multi-population Cuckoo Search algorithm to segment the tumor part and rectangular shape is preferred for processing the segmentation and it yields better segmentation accuracy.

Zhang et al. [6] identified the pathological brain from the normal brain by applying fractional Fourier entropy with multi-layer perception classifier and achieved 99.53% segmentation accuracy. A study by Nilanjan Dey [7] investigates the Cuckoo Search Optimizations and finds the tumor part in MR brain images based on the contrast of the input image. Modified tracking algorithm and Hybrid Center Weighted Median Filter are used for pre-processing and Markov random field is used as the central pixel for Cuckoo Search.

Brain tumor detection can be divided into three types, namely semi-automatic, fully-automatic and expert segmentation. Jin Liu et al. [8] used multi parameter watershed segmentation to detect 2D and 3D MRI brain images. Ramathilagama et al. [9] recommended using distance maximum algorithm to reduce the number of iterations before evaluating the segmented MRI brain images. Vishnuvarthan [10] applied fuzzy inference rules to segment the tumor part of MRI brain images in minimum time. Krishnapriya [11] applied Fuzzy C-Means (FCM) clustering method based on the region growing approach to classify the pixels into various segments. FCM is an unsupervised clustering technique suitable for all images including medical images of various modalities [12]. Serra [13] compared FCM and improved FCM with MRI brain tumor and concluded that CPU processing time is reduced when improved FCM clustering is applied to the input image,

but in some cases, it does not guarantee the continuation of boundaries. Sudha [14] extracted the features of texture, histogram, radial, and shape of the breast cancer by applying enhanced Cuckoo Search technique, and it was compared with harmony search and Cuckoo Search yielded better accuracy. Osman et al. [15] suggested FCM clustering for identifying the presence of abnormalities in the breast including mass lesions and Micro Calcification Clusters. Gubern-Merida et al. [16] found the breast density and fibro-glandular tissues of MR breast images using ATLAS segmentation and proved its reliability by measuring the density from MR and Mammogram images. Ahmed et al. [17] applied multi-channel Markov field along with belief propagation and conditional mutual information for segmenting the tumor region in the breast. Cascio et al. [18] proposed neural network concept for classifying the lesions of breast cancer by applying contour based searching segmentation. Panetta et al. [19] applied NLUM (Non-Linear un-sharp masking) scheme to enhance mammogram contrast for detecting the tumor in mammogram images. There is a need for improving the performance of the segmentation with less time by testing the abnormal parts present in MR brain and breast images. For achieving better performance of medical image segmentation, Kapur's entropy [20], which is suitable for segmenting the tumor part in both MR brain and breast images is used, as it maximizes the summation of entropy based on information theory. It always produces the positive probability and global maximum value and provides better average scores than any other non-destructive sample images.

Kavitha used Genetic segmentation with SVM classifier [21] to classify the tumor as benign or malignant with limited set of images. In [22] entropy, features are combined with LSDA to identify normal, FLD and cirrhotic liver from US images and yields 97% accuracy with PNN classifier. Mahalakshmi [23] used MR Brain DICOM images and segment the axial and coronal plane using PSO and extracted the tumor part by filtering methods. It was observed that the average elapsed time for segmentation ranges from 15 to 17 s and proved that the coronal plane takes less time than the axial plane for segmentation. Nagesh et al. [24] utilized charged fluid model method to segment the region of interest using Ostu's algorithm for both MR brain and breast images. In their study, they focus only region of interest of charged fluid model and segmentation takes 0.326 s. Mookiah et al. [25] discussed the importance of GA and Particle swarm Optimization (PSO) in detecting the hard exudates, blood vessels, textures and entropies in diabetic retinopathy images.

Higher order spectra (HOS) fuzzy entropy was applied by Rajendra et al. [26] which are used to classify the normal and abnormal fatty liver diseases. Muthu Rama Krishnan et al. [27] suggested discrete wavelet transform (DWT) coefficients like energy, entropy, Gini index and various statistical moments like mean, variance, skewness, Kurtosis are applied to classify age related macular degeneration. In recent research studies [28,29] Kapur's Entropy function has been used to segment the gray level images and RGB images with the threshold values (2,3,4,5) and performed segmentation with minimum duration. FCM is a soft clustering approach, which minimize the objective function and iterations than other clustering

algorithms. The major drawback of FCM is that numbers of clusters are not known in advance for finding cluster centroids is discussed by Ajala et al. [30]. PSO is a global optimization technique, which simulates the behavior of birds flocking. It solves number of medical applications more efficiently. Daamouche et al. [31] suggested PSO technique for feature extraction and select the informative features obtained by morphological profiles for classification. In some applications PSO leads high-dimensional space and has a low convergence rate in the iterative process. Many researchers focus single modal of image for processing, but we combine the working principle of Kapur's entropy with CS optimization and morphological filters for multimodal images. Ratna Raju [32] applied Bayesian fuzzy clustering approach for segmentation and harmony crow search optimization with multi SVNN classifier for classification and produces 93% of classification accuracy Jyotsna Dograa [33] utilized k-means clustering and graph cut algorithm for segmenting the MR brain tumor using centriod points for initialization and applied various quantitative measures to ensure the accuracy of segmentation. Odelin Charron et al. [34] applied deep network approach to detect and segment the brain metastases on multimodal MRI. Aboul EllaHassanien et al. [35] introduced a hybrid system of adaptive ant based clustering for segment the tumorous part of breast and classify the benign and malignant images with multilayer perceptron neural network approach. Ball [36] reported the importance of BI-RADS used discriminating benign from malignant lesions Mammogram breast images.

2.   Methods and materials

2.1.   Scope of our work

The main goal of our study is to combine two different methodologies into single automated system to segment the tumor part present in both MR brain and breast images. No other researchers applied a single method to segment the multimodal images, with same parameters with different modalities of images. Our automated algorithm is very helpful for a radiologist to understand the severity of the diseases in T1 axial, T2 axial, T1 enhanced, T2 enhanced images for MR brain, post processed and T1 post contrast images for breast. Our algorithm assists the radiologist to understand and prevent the severity of diseases in early stage. CS, FCM and PSO algorithms are competitive optimization techniques and are used for many medical image processing techniques. Segmentation parameters are applied to validate the performance of our algorithm with FCM and PSO. We compare the accuracy and computational time with FCM, PSO and CS, and we proved that CS with morphological filters is suitable for segmenting the both modalities.

2.2.   Details of image dataset

In this study, we have used various clinical images such as MR brain Images and MR breast cancer images for testing and validating our technique.

2.2.1.   MR brain images
MR images are acquired from an MRI scanner and some of their sequences such as T1, T2 weighted axial images were used. Images are also obtained from the online database like Brain Tumor Scans (BRATS 2013), Harvard's brain web database and from clinical database.

2.2.2.   MR breast images
Breast cancer is a common disease that has increased death rate worldwide. Hence, there is a need to detect the benign stage of breast cancer. We have used images from various online databases for MR Breast images like Reference Image Database to Evaluate Therapy Response (RIDER) and Breast Imaging Reporting and Database System (BIRADS) [21].

2.3.   Image analysis

Our proposed method is described below:

> Step 1: Convert the input image of size 256×256 into grayscale image.
> Step 2: Apply Kapur's entropy based Cuckoo Search Optimization search technique to segment the tumor part, without any preprocessing. We apply only Kapur's entropy to maximize the global threshold.
> Step 3: Apply morphological reconstruction operations to segment tumor part with accurate size by removing the unwanted pixels [22].
> Step 4: Test the images using the segmentation metrics like as MSE, PSNR, Jaccard Index, Hausdorff distance, Entropy, Precision, Recall, accuracy, and Computational time.
> Step 5: Compare the derived parameters with the parameters obtained by FCM and PSO segmentation and its computation time for extraction. Fig. 1 shows an overview of the proposed work.

2.4.   Kapur's entropy

Sathya et al. [37] applied Kapur's method to maximize the entropy measures of the segmented histogram by applying the centralized distribution which cannot be achieved easily using a bilateral gray level histogram. Maximum threshold value is fixed based on the gray level values between background and tumor part. Kapur's entropy was computed as explained below.

The probability of each gray level i is the relative occurrence frequency of the gray level i normalized by the total number of gray levels

$$P_i = \frac{h_i}{\sum_{i=0}^{L-1} h_i} \quad i = 0, \ldots, L-1 \tag{1}$$

$$H_0 = -\sum_{i=0}^{t_1-1} \left(\frac{p_i}{w_0}\right) \log_2 \left(\frac{p_i}{w_0}\right)$$

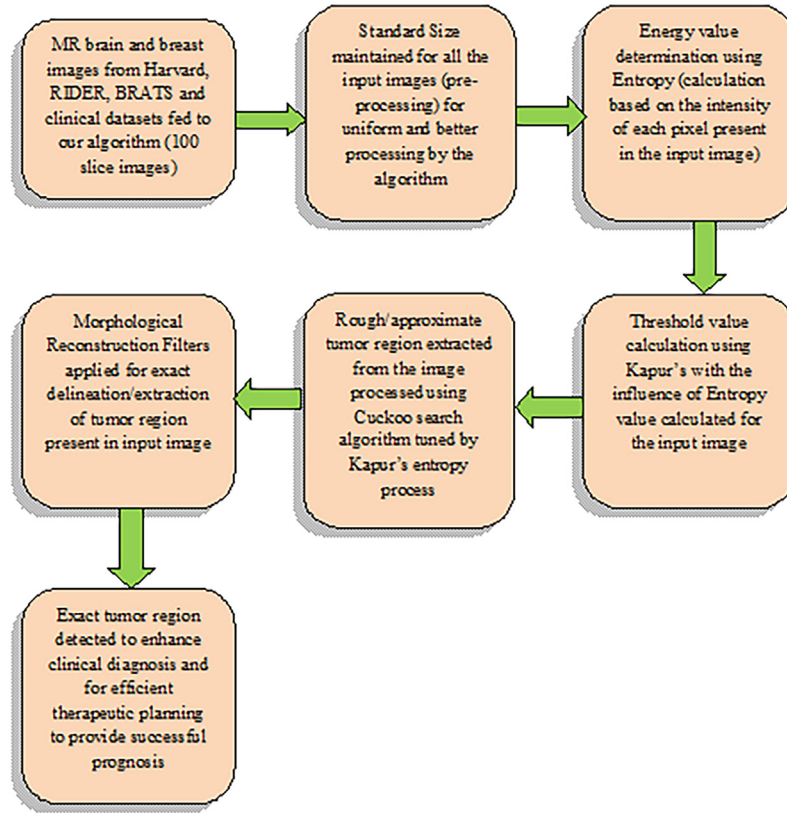$$H_1 = -\sum_{i=t_1}^{t_2-1} \left(\frac{p_i}{w_1}\right) \log_2 \left(\frac{p_i}{w_1}\right)$$

Fig. 1 – Flow Diagram of our proposed method.

$$H_j = -\sum_{i=t_j}^{t_{j+1}-1} \left(\frac{p_i}{w_j}\right) \log_2 \left(\frac{p_i}{w_j}\right)$$

$$H_m = -\sum_{i=t_m}^{N-1} \left(\frac{p_i}{w_m}\right) \log_2 \left(\frac{p_i}{w_m}\right)$$

$$w_0 = \sum_{i=0}^{t_1-1} p_i; \quad w_1 = \sum_{i=t_1}^{t_2-1} p_i;$$

$$w_j = \sum_{i=t_j}^{t_{j+1}-1} p_i; \quad w_m = \sum_{i=t_m}^{N-1} p_i; \tag{2}$$

where $H_0, H_1, \ldots, H_m$ represents the entropy values for $m+1$ regions and p_i represents the probability of the pixel intensity values with range from 0 to 255 and N represents the total number of intensity values in the MR brain and breast input image.

2.5. Cuckoo Search Optimization

It is one of the meta-heuristic optimization techniques which describes the reproductive policy of cuckoo species [2]. Naturally, cuckoos lay its eggs in other bird's nest or destroy host eggs or build a new nest at another place when the host eggs are destroyed. The objective of this technique is to use the

best solution which has a more hatching probability count and replacement of other eggs which will not provide a better result. When cuckoo birds search the nest, they use the concept of Levy Flight [1]. Levy Flight involves a random walk in which step length is obtained from the Levy distribution. Cuckoo Search Optimization contains the following three rules

- An egg will be laid by a cuckoo at a time and dumps its egg in a randomly chosen nest
- Select the best nests with high quality of eggs that will carry to the next generations
- Total number of host nest is fixed and with the help of probability Pa ∈ [0,1] the host can be able to find the number

Table 1 – Parameters used in the Cuckoo Search Optimization for our proposed method.	
Number of nests (N)	20
Minimum eggs	2
Maximum eggs	5
Maximum iterations	70
Clusters	2
Motion coefficients	2
R-coefficients	4
Mutation probability (Pa)	0.5
Lower bound	5
Upper bound	300
Scale factor (beta)	1.5
Step size (alpha)	0.01

of eggs laid by the cuckoo. For generating new solutions, levy flight is performed using Eq. (3)

$$x_i^{(t+1)} = x_i^{(t)} + \alpha \oplus \text{Levy}(\lambda) \tag{3}$$

where $\alpha > 0$ is step size scaling factor, $x_i^{(t)}$ represents the initial location, $x_i^{(t+1)}$ represents the updated location and $\oplus$ represents the entry wise multiplication. The levy distribution function is given as

$$Le(\lambda) = t^{-\lambda} \quad 1 < \lambda \le 3 \tag{4}$$

$$\sigma^2(t) \sim t^{2-\beta} \quad 1 \le \beta \le 2 \tag{5}$$

Eq. (5) represents the nonlinear relationship of variance of levy flight. This process continues till it reaches the optimal solution. A complete pseudo code for the Lévy flight-based CS algorithm method and the parameter used for implementation is mentioned in Table 1.

Lévy Flight-based CS algorithm

1: Initialize a population of n host nests at random
2: while stopping criteria not met do

3: Obtain a cuckoo xi at random by Levy flights

4: Choose a nest xj randomly
5: if f(xi) better than f(xj) then

6: Replace j by the new solution
7:   end

8: Abandon a fraction of the worse nests and create new ones using Levy flights
9: end

2.6. Morphological reconstruction filters

Cuckoo Search Optimization segments the abnormal part in MR brain and MR breast images with some additional pixels that are irrelevant. Based on the suggestions from the radiologist, some patches are removed by applying the morphological reconstruction filters which use mathematical morphology. Mathematical morphology is used to describe the shapes of given object using set theory. It is also used to investigate the relationship between input image with structuring elements like erosion and dilation [38,39].

Table 2 – Performance measures of our proposed work.					
S.No.	Image No.	Eccentricity	Entropy	Jaccard Index	Hausdorff distance
S1	T2 Axial	0.856	0.024	0.982	0.23
S2	T2 Axial	1.314	0.036	0.970	0.25
S3	T2 Axial	0.640	0.048	0.984	0.34
S4	T2 Axial	0.889	0.069	0.963	0.22
S5	T2 Axial	1.155	0.300	0.946	0.45
S6	T2 Axial	1.456	0.420	0.947	0.47
S7	T2 Axial	1.342	0.045	0.921	0.34
S8	T2 Axial	1.325	0.310	0.967	0.36
S9	T2 Axial	1.452	0.460	0.961	0.37
S10	T2 Axial	1.230	0.023	0.782.	0.52
S11	T1 Axial	1.560	0.181	0.744	0.25
S12	T1 Axial Post Contrast	10.73	0.179	0.720	0.45
S13	T1 Coronal Post Contrast	0.919	0.134	0.920	0.42
S14	T1 axial Post Contrast	0.154	0.226	0.963	0.49
S15	T1 Axial Post Contrast	0.897	0.014	0.974	0.34
S16	T1 Axial	0.871	0.145	0.981	0.42
S17	T1 Axial	0.982	0.167	0.989	0.32
S18	Post processed	0.527	0.139	0.942	0.27
S19	Post processed	0.674	0.219	0.936	0.42
S20	Post processed	0.124	0.312	0.962	0.38
S21	Post processed	0.121	0.204	0.971	0.34
S22	Post processed	0.912	0.147	0.947	0.42
S23	Post processed	0.547	0.451	0.775	0.34
S24	Post processed	0.9821	0.412	0.732	0.24
S25	Post contrast	0.527	0.024	0.882	0.31
S26	Post contrast	0.671	0.072	0.961	0.42
S27	Post contrast	0.543	0.014	0.906	0.34
S28	Post contrast	1.330	0.144	0.974	0.36
S29	T1 Post contrast	1.460	0.133	0.982	0.37
S30	T1 Post contrast	1.660	0.185	0.976	0.42
S31	T1 Post contrast	1.230	0.103	0.984	0.33

Dilation of a binary image A and B can be denoted as:

$$A \oplus B = \{z | (B) \cap A \neq \phi\} \tag{6}$$

Erosion shrinks the objects and defined as:

$$A \Theta B = \{z | (B) \cap A^c \neq \varphi\} \tag{7}$$

where A is the input image and B is the structuring element applied to the input image. The Opening of input A by B is defined as erosion followed by dilation and it is represented as:

$$A \circ B = (A \Theta B) \oplus B \tag{8}$$

Closing is defined as dilation followed by erosion and it is denoted as:

$$A \bullet B = (A \oplus B) \Theta B \tag{9}$$

where small holes in the foreground pixels that are smaller than S will be filled. Structural element plays a vital role in morphological operation. In our method, we prefer to use disc as the structural element and its size is 5 × 5 is fixed for both modalities, because it runs faster, when the structuring element uses approximation. So, we prefer disc structure for morphological operations

3. Performance measures

The performance of our proposed method is validated using various measures like Eccentricity, Entropy, Jaccard Index, Hausdorff Distance, Mean Square Error (MSE), Peak Signal to Noise (PSNR), Precision, Recall and Accuracy. The Accuracy of our segmentation result is measured by comparing the CS segmented images with expert segmentation images.

3.1. Eccentricity

Eccentricity provides ratio using maximum and minimum axis by using bounding rectangle method with width and height of rectangular boundary is denoted as:

$$E = 1 - \frac{\text{Length}}{\text{Width}} \tag{10}$$

3.2. Entropy

Entropy measures the average amount of missing information of given gray scale image [39]. The probability values p_i is defined as:

$$\text{Entropy} = -\sum_{i=1}^{n} p_i \log_b(p_i) \tag{11}$$

3.3. Jaccard index

Jaccard Index calculates the similarity between input and ground truth image [40]. The numerator represents the

similarity and denominator represents both similar and dissimilar pixels

$$J(A, B) = \frac{S(A \cap B)}{S(A \cup B)} \tag{12}$$

where A is the original image and B is the segmented image.

3.4. Hausdorff distance

Hausdorff is a metric that measures the Hausdorff distance between all feature points of input (A) and output image (B) [14,41,42] and the forward and backward distance of h(A,B) and h(B,A) is as follows:

$$H(A, B) = \max(h(A, B), h(B, A)) \tag{13}$$

3.5. Mean Square Error (MSE)

The MSE is used to find the accumulative square error between the input image $F(i, j)$ and the segmented image $S(i, j)$,

$$\text{MSE} = \frac{1}{mn} \sum_{i=0}^{m-1} \sum_{j=0}^{n-1} [F(i, j) - S(i, j)]^2 \tag{14}$$

Table 3 – MSE and PSNR comparison of our proposed work with FCM, PSO and CS.

Image No.	MSE values			PSNR values		
S1	FCM	PSO	CS	FCM	PSO	CS
S2	0.021	0.021	0.011	42.1	23.95	46.41
S3	0.032	0.061	0.003	36.85	30.13	32.87
S4	0.041	0.049	0.039	33.89	34.13	32.17
S5	0.034	0.03	0.044	35.85	32.54	31.17
S6	0.034	0.062	0.032	35.98	25.87	38.96
S7	0.032	0.832	0.026	35.13	26.92	38.82
S8	0.088	0.091	0.081	26.36	29.74	27.84
S9	0.022	0.112	0.014	44.62	23.95	37.27
S10	0.039	0.036	0.021	40.39	35.09	31.37
S11	0.032	0.035	0.032	31.88	36.54	35.88
S12	0.011	0.041	0.073	27.69	35.87	32.62
S13	0.079	0.165	0.003	27.35	19.16	51.94
S14	0.09	0.083	0.035	35.45	26.68	39.78
S15	0.036	0.132	0.021	35.39	19.21	39.5
S16	0.032	0.071	0.023	35.98	27.57	32.51
S17	0.101	0.045	0.021	30.39	32.04	47.34
S18	0.154	0.061	0.073	31.03	30.03	31.35
S19	0.142	0.211	0.055	31.38	17.05	34.08
S20	0.001	0.221	0.003	47.7	17.01	58.54
S21	0.005	0.162	0.001	39.64	20.04	40.87
S22	0.026	0.154	0.018	45.82	20.69	36.32
S23	0.012	0.06	0.005	31.52	30.03	43.44
S24	0.001	0.218	0.006	42.1	17.08	48.11
S25	0.056	0.073	0.041	31.01	27.82	33.71
S26	0.038	0.037	0.032	33.77	34.83	36.31
S27	0.031	0.085	0.024	32.05	26.85	41.56
S28	0.066	0.102	0.042	28.28	30.12	33.62
S29	0.049	0.085	0.022	21.05	26.85	37.96
S30	0.105	0.06	0.041	31.32	30.03	32.17
S31	0.102	0.012	0.045	20.8	25.01	31.63

where m and n represent row and columns used in the input image.

3.6. Peak Signal to Noise (PSNR)

The PSNR measure calculates the peak signal-to-noise ratio between input and segmented image

$$PSNR = 10 * \log 10 \left(\frac{255}{\sqrt{MSE}} \right) \qquad (15)$$

3.7. Precision and recall

Precision and recall have been commonly used in recent literature to measure how well the segmented image corresponds to the input image [43]. Recall can be interpreted as the number of true positive parts segmented by an algorithm, while precision evaluates the tendency of an algorithm for false positives. Once all input and output segmentation are matched using the proposed method, Precision and Recall are computed by:

$$Precision = \frac{t_p}{t_p + f_p} \qquad (16)$$

$$Recall = \frac{t_p}{t_p + f_n} \qquad (17)$$

The precision and recall index examines the pair-wise relationships in the segmentation.

Accuracy is defined by:

$$Accuracy = 2 * \frac{t_p}{t_p + f_n} \qquad (18)$$

where t_p (True Positive) represents the correct segmentation of tumor part, t_p (False positive) represents normal region present in the input image identified wrongly as tumor region, f_n (False negative) represents the wrongly segmented tumor region and t_n (True Negative) represents the correct segmentation of non-tumorous part.

4. Results and discussion

Table 2 provides the details of performance evaluation measures like Eccentricity, Entropy, Jaccard Index, Hausdorff distance of our proposed work. These measures are helpful for comparing the segmentation accuracy of our method with

Table 4 – Efficiency in terms of Precision, Recall and Accuracy measures of CS.			
Image No.	Precision	Recall	Accuracy
S1	94.2	99	96.5
S2	97	97.2	97.5
S3	96.7	97.3	97.5
S4	92.7	97.2	96.9
S5	95.7	98.9	97.3
S6	96.3	95.7	96.5
S7	96.3	98	97.7
S8	95	100	96.6
S9	91.7	100	95.6
S10	94.1	92.7	93.4
S11	98.8	97.9	98.4
S12	96	99	97.5
S13	96.1	98	97.6
S14	95.7	98.9	97.3
S15	91.9	98.5	94.9
S16	95	100	96.3
S17	97.5	96.7	97.5
S18	97.1	99	99
S19	97.2	97	97.1
S20	96.3	100	97.1
S21	85.1	98.9	91.8
S22	97.7	97.8	97.8
S23	91.6	98.8	95.1
S24	100	94.5	97
S25	95.7	98.1	97
S26	99	96.1	97.5
S27	94.1	92.7	93.5
S28	100	94.5	97.1
S29	89.7	97	97
S30	95.5	98.8	97
S31	94.2	99	96.5
Average	95.29	97.65	96.63

Table 5 – Computational time comparison between FCM, CS and PSO.			
Image No.	FCM	PSO	CS
S1	3.02	4.17	3.26
S2	3.84	4.67	2.67
S3	3.38	3.61	2.97
S4	2.43	3.02	1.07
S5	2.97	3.93	2.76
S6	4.16	4.52	3.01
S7	3.76	4.28	2.13
S8	4.19	4.9	3.14
S9	3.72	4.83	2.69
S10	2.87	4.33	2.75
S11	2.43	4.26	2.35
S12	3.44	3.98	3.36
S13	3.09	4.09	2.68
S14	2.81	4.18	2.08
S15	3.01	3.29	2.01
S16	3.14	4.23	2.03
S17	2.76	4.16	3.16
S18	2.65	3.87	2.86
S19	3.3	4.17	3.06
S20	2.65	3.08	2.76
S21	3.21	4.18	3.13
S22	2.97	4.04	2.87
S23	2.76	4.65	2.09
S24	3.998	4.22	3.82
S25	3.16	3.27	3.02
S26	3.87	4.18	3.21
S27	3.7	3.99	3.65
S28	3.71	4.16	2.81
S29	2.42	3.89	2.11
S30	2.19	4.17	2.13
S31	2.89	3.98	2.08
Average	3.18	4.07	2.7

existing methodology for future researchers. Jaccard Index provides the vital information about the commonality between input image and segmented image.

Similarity of both input and segmented output values is 0 ensures no overlap. Hausdorff distance represents the minimal distance between the boundaries of original and segmented images. The values of all images have the average Hausdorff distance as 0.2.

Table 3 provides the MSE and PSNR values of our proposed work FCM PSO and CS algorithm. It shows that Kapur's entropy based cuckoo search segmentation produces average MSE value of 0.028 which was compared with FCM and PSO. An average of PSNR value produced by FCM, PSO and CS are 32.99, 26.22 and 36.64. The CS algorithms PSNR value is high compared with FCM and PSO and its value lies between 30 and 50 dB. If the PSNR value is high and MSE value is between 0 and 1 proves that segmented output image noise is very low.

The efficiency of our work is validated by applying precision-recall and accuracy values and is mentioned in the Table 4, Accuracy is measured between the input image and expert segmented output images, our proposed method yields average of 97% accuracy for both modalities

Time taken for segmenting the tumor part in brain and breast images is measured in seconds. Table 5 shows the
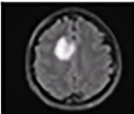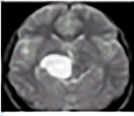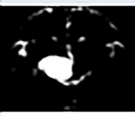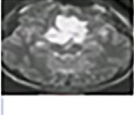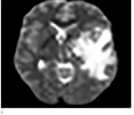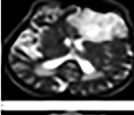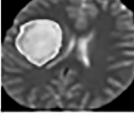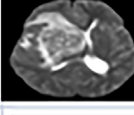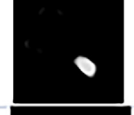
Image No	Image Source	Image Type	Input images	FCM output	PSO	Kapurs based CS with Morphological filters
S1	Harvard Dataset	T2 Axial				
S2	Harvard Dataset	T2 Axial				
S3	BRATS	T2 Axial				
S4	BRATS	T2 Axial				
S5	Harvard Dataset	T2 Axial				
S6	Harvard Dataset	T2 Axial				
S7	BRATS	T2 Axial				
S8	BRATS	T2 Axial				
S9	BRATS	T2 Axial				
S10	BRATS	T2 Axial				

Fig. 2 – T2 Axial MR brain images.
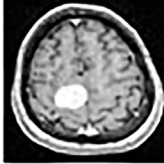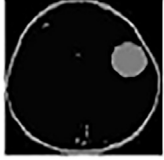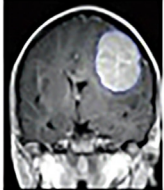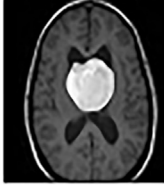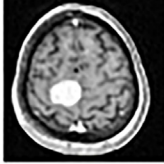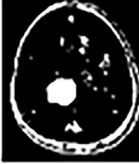
Image No	Image Source	Image Type	Input Images	FCM Output	PSO	Kapurs based CS with Morphological filters
S11	Clinical database	T1 Axial				
S12	BRATS	T1 Axial Post Contrast				
S13	BRATS	T1 Coronal Post Contrast				
S14	BRATS	T1 Axial Post Contrast				
S15	BRATS	T1 Axial Post Contrast				
S16	BRATS	T1 Axial				
S17	Clinical database	T1 Axial				

Fig. 3 – T1 Axial, T1 post contrast and T1 coronal post contrast MR brain images.
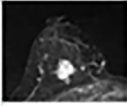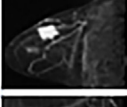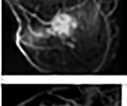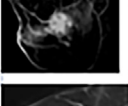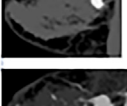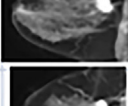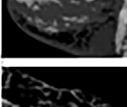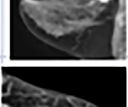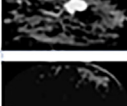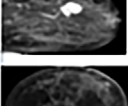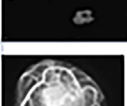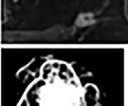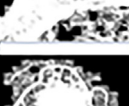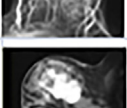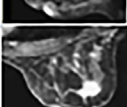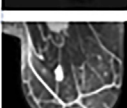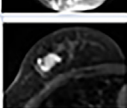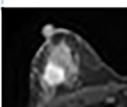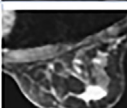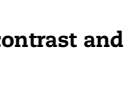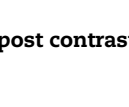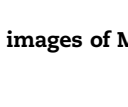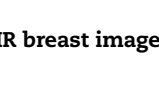
Image No	Image Source	Image Type	Input images	FCM output	PSO	Kapurs based CS with Morphological filters
S18	BIRADS	Post Processed				
S19	BIRADS	Post Processed				
S20	BIRADS	Post Processed				
S21	BIRADS	Post Processed				
S22	Clinical dataset	Post Processed				
S23	BIRADS	Post Processed				
S24	BIRADS	Post Processed				
S25	BIRADS	Post Contrast				
S26	BIRADS	Post Contrast				
S27	Clinical dataset	Post Contrast				
S28	BIRADS	Post Contrast				
S29	BIRADS	T1 Post Contrast				
S30	BIRADS	T1 Post Contrast				
S31	BIRADS	T1 Post Contrast				

Fig. 4 – Post processed, T1 post contrast and post contrast images of MR breast images.
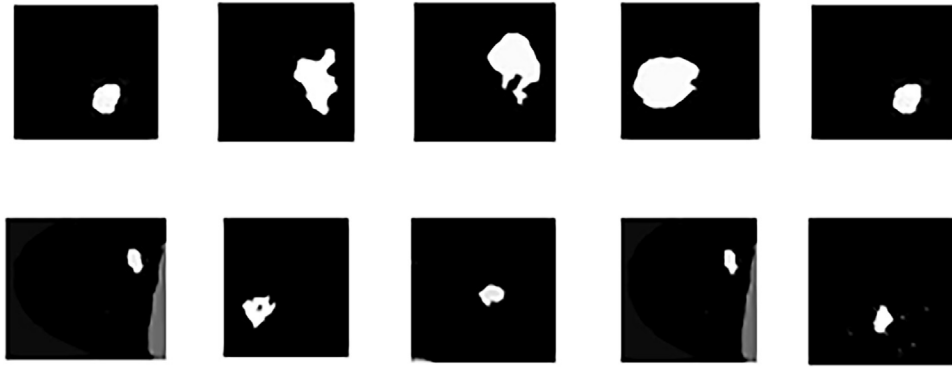
Fig. 5 – Ground truth images of MR brain and breast images.
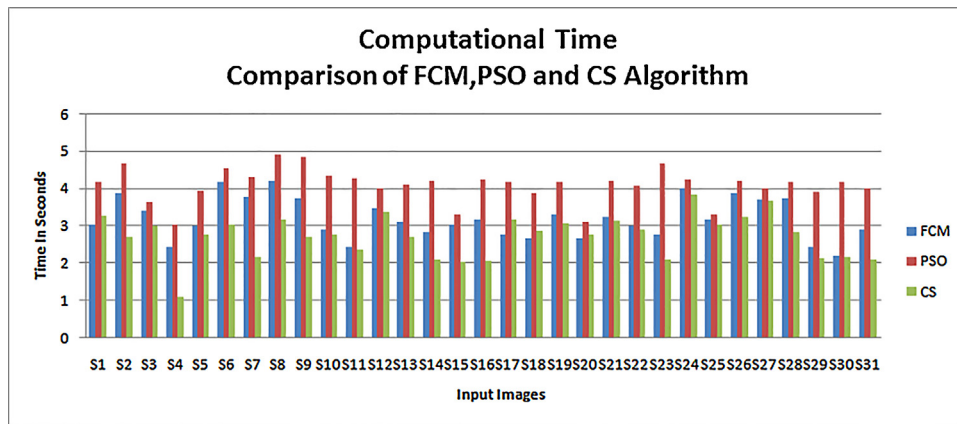
Fig. 6 – Computational time comparison between FCM, PSO and CS algorithm.
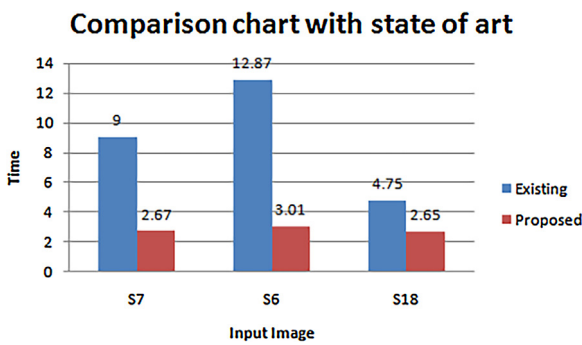
Fig. 7 – Computational time comparison among existing techniques.

computational time comparison between FCM, PSO and Kapur's entropy based cuckoo search segmentation method.

Figs. 2 and 3(S1–S17) contains T2 axial, T1 axial, T1 post contrast and T1 Coronal Post Contrast images collected from online dataset like BRATS, Harvard's dataset, and clinical dataset, which enhance the visualization of the brain tumor of the patients aged from 5 to 35. Figs. 2 and 3(a) contains input gray scale image with the size of 256 × 256 and in Figs. 2 and 3 (b) contains FCM segmentation images and Figs. 2 and 3(c) contains PSO based Segmentation output and Figs. 2 and 3(d)

contains our proposed Kapur's entropy-based CS algorithm with morphological reconstruction filters.

Fig. 4(S18–S31) contains post processed images and T1 post contrast and post contrast images of MR breast images collected from online dataset like BI-RADS and clinical dataset. The use of post processed images is to view the tumor part clearly and it is easy to segment the tumor part from post processed images. From the output images it was proved that our proposed method segments the tumor accurately than FCM and PSO segmentation method.

Fig. 5 shows some samples of MR brain and breast image manually segmented by expert radiologist. The accuracy of our proposed method is calculated between obtained segmented output and manual expert segmentation. From the sample ground, our proposed method ensures 97% of accuracy.

Fig. 6 shows the Computational time comparison between FCM, PSO and CS algorithm. It was observed that our proposed method takes overall average of minimum 4 ms for segmenting both modalities of all input images and comparatively better then FCM and PSO method.

Comparison of time of other state of art methods [9,10,14] is mentioned in Fig. 7. It shows that our work is suitable for segmenting various types of tumor in MR brain and breast images. From the Comparison chart, we observe that our

proposed method is suitable for determining the effective segmentation for finding the malignant tumor part present in brain and breast images within a short period. This is also helpful for radiologist to prevent the growth of tumor in earlier stages or removing the tumor. For implementation, we used MATLAB software R2012b with Intel Core(TM) i5-4210U Processor of 1.70 GHz clock speed and 4GB RAM and 64-bit operating system for processing and validating our results.

5. Conclusion

In this study, we have tested a novel common technique with two modalities based on Kapur's entropy and cuckoo search segmentation and morphological reconstruction filters. This technique required minimum 4 ms for segmenting the tumor part of MR brain and breast images with various images types like T2 axial, T1 axial, post processed images and T1 post contrast enhanced images which will be helpful for radiologist to analyze the severity of tumors. From the MSE and PSNR values it was proved that the segmentation results obtained by the proposed algorithm have good immunity toward noise interference. The accuracy rate of our proposed method is far better than FCM and PSO algorithm. However, the drawback of this method lies in applying same parameters for both modalities which is not in practice currently. By applying the same structuring element for both brain and breast is not flexible for some images. HOS is mainly focused on classification of tumor as benign or malignant; however for segmenting the tumor in post processed breast images, it leads poor result. So we are not applied HOS features for our proposed method. In our future work, we wish to focus the same approach with various classification techniques like SVM, neural network along with optimization algorithms like whale optimization and Bat optimization etc.

Author contributions

R. Sumathi contributed to image analysis, software design, development techniques, classification accuracy, and drafting the article; M. Venkatesulu contributed to concept of work, drafting the article, critical revision of the article, and final approval; Sridhar P. Arjunan contributed to contributed to concept of work, designing, selection of analytical tools, critical revision of an article.

Acknowledgement

REFERENCES

[1] Yang XS, Deb S. Cuckoo search via Levy flights. Proceedings of World Congress on Nature & Biologically Inspired Computing (NaBIC 2009 India) 2009;210–4.

[2] Yang X, Deb S. Engineering optimization by Cuckoo search. Int J Math Model Num Optim 2010;1:330–43.

[3] Roushdy M. Comparative study of edge detection algorithms applying on gray scale noisy image using morphological filters. Int J Graph Vis Image Process 2006;6:17–23.

[4] Pratheeba S, Sheeja Kumari V. Healthy and pathological tissue classification in MRI brain images using HCSONN algorithm. Int J Innov Res Sci Eng Technol 2016;5.

[5] Ilunga-Mbuyamba E, Cruz-Duarte JM, Avina-Cervantes JG, Correa-Cely CR, Lindner D, Chalopind C. Active contours driven by Cuckoo Search strategy for brain tumor images segmentation. Expert Syst Appl 2016;56:59–68.

[6] Zhang Y, Sun Y, Phillips P. A multilayer perception based smart pathological brain detection system by fractional Fourier entropy. J Med Syst 2015;40:173–84.

[7] Dey N, Ashour AS, Beagum S, Pistola DS, Gospodinov M, Gospodinova EP, et al. Parameter optimization for local polynomial approximation based intersection confidence interval filter using genetic algorithm: an application for brain MRI image de-noising. J Imaging 2015;1:60–84.

[8] Liu J, Li M, Wang J, Wu F, Liu T, Pan Y. A survey of MRI-based brain tumor segmentation methods. Tsinghua Sci Technol 2014;19:578–95.

[9] Ramathilagama S, Pandiyarajan R, Sathya A, Devi R, Kannan SR. Modified fuzzy c-means algorithm for segmentation of T1–T2-weighted brain MRI. J Comput Appl Math 2011;235:1578–86.

[10] Vishnuvarthan G, Pallikonda Rajasekaran M. Segmentation of MR brain images for tumor extraction using fuzzy inference systems. Curr Med Imaging Rev 2013;9:2–6.

[11] Krishna Priya R, Thangaraj C, Kesavadas C. Fuzzy C-means method for color image segmentation with L*U*V colour transformation. IJCSI Int J Comput Sci 2011;1. 1694-0814.

[12] Bezdek JC, Hall LO, Clarke LP. Review of MR image segmentation techniques using pattern recognition. Med Phys 1993;20:1033–48.

[13] Serra J. Image analysis and mathematical morphology. New York Academic; 1982.

[14] Sudha MN, Selvarajan S. Selection based on enhanced Cuckoo Search for breast cancer classification in mammogram image. Feature Circuits Syst 2016;7:327–38.

[15] Osman MA, Darwish A, Ghalwash AZ, Hassanien AE. Enhanced breast cancer diagnosis system using fuzzy clustering means approach in digital mammography. Handbook of research on machine learning innovations and trends. USA: IGI; 2017.

[16] Gubern-Merida A, Kallenberg M, Mann RM, Mart R, Karssemeijer N. Breast segmentation and density estimation in breast MRI: a fully automatic framework. IEEE J Biomed Health Inform 2015;19:349–57.

[17] Ashraf AB, Gavenonis CS, Daye D, Mies C, Rosen MA, Kontos D. Multichannel Markov random field framework for tumor segmentation with an application to classification of gene expression based breast cancer recurrence risk. IEEE Trans Med Imaging 2013;32:637–48.

[18] Cascio D, Fauci F, Magro R, Raso G, Bellotti R, De Carlo F, et al. Mammogram segmentation by contour searching and mass lesions classification with neural network. IEEE Trans Nucl Sci 2006;53:2827–33.

[19] Panetta K, Zhou Y, Agaian S, Jia HW. Nonlinear Unsharp masking for mammogram enhancement. IEEE Trans Inf Technol Biomed 2011;15:918–28.

[20] Kapur JN, Sahoo PK, Wong AKC. A new method for gray-level picture thresholding using the entropy of the histogram. Comput Vis Graph Image Process 1985;29:273–85.

[21] Kavitha AR, Chitra L, Kanaga R. Brain tumor segmentation using genetic algorithm with SVM classifier. Int J Adv Res Electr Electron Instrum Eng 2016;5:1468–71.

[22] Hu Q, Yu D. Entropies of fuzzy indiscernibility relation and its operations. Int J Uncertain Fuzziness Knowl-Based Syst 2004;12:575–89.

[23] Mahalakshmi S, Velmurugan T. Detection of brain tumor by particle swarm optimization using image segmentation. Indian J Sci Technol 2015;8:13–9.

[24] Vadaparthi N, Yarramalle S, Suvarna Kumar G, Vamsee Krishna V. An improved medical image segmentation using charged fluid model. Int J Eng Res Appl 2012;2:666–8.

[25] Mookiah MRK, Rajendra Acharya U, Martis RJ, Chua CK, Lim CM, Ng EYK, et al. Evolutionary algorithm based classifier parameter tuning for automatic diabetic retinopathy grading. A hybrid feature extraction approach. Knowl-Based Syst 2013;39:9–22.

[26] Rajendra Acharya U, Fujita H, Koha JEW, Sudarshan VK, Vijayananthan A, Yeong CH, et al. Automated characterization of fatty liver disease and cirrhosis using curvelet transform and entropy features extracted from ultrasound images. Comput Biol Med 2016;79:250–8.

[27] Krishnan Mookiah MR, Rajendra Acharya U, Koh JEW, Chua CK, Tan JH, Chandran V, et al. Decision support system for age-related macular degeneration using discrete wavelet transform. Med Biol Eng Comput 2014;52:781–96.

[28] Suresh Manic K, Krishna Priya R, Rajinikanth V. Image multithresholding based on Kapur/Tsallis entropy and firefly algorithm. Indian J Sci Technol 2016;9:1–6.

[29] Sri Madhava Raja N, Vishnupriya R. Kapur's entropy and Cuckoo Search algorithm assisted segmentation and analysis of RGB images. Indian J Sci Technol 2016;9:1–6.

[30] Ajala Funmilola A, Oke OA, Adedeji TO, Alade OM, Adewusi EA. Fuzzy k-c-means clustering algorithm for medical image segmentation. J Inf Eng Appl 2012;2:21–32.

[31] Daamouche A, Melgani F, Alajlan N, Conci N. Swarm optimization of structuring elements for VHR image classification. IEEE Geosci Remote Sens Lett 2013;10:1334–8.

[32] Ratna Raju A, Suresh P, Rajeswara Rao R. Bayesian HCS-based multi-SVNN: a classification approach for brain tumor segmentation and classification using Bayesian fuzzy clustering. Biocybern Biomed Eng 2018;38:646–60.

[33] Dograa J, Jaina S, Sooda M. Segmentation of MR images using hybrid k mean-graph cut technique. Procedia Comput Sci 2018;132:775–84.

[34] Charron O, Lallement A, Jarnet D, Noblet V, Clavier J-B, Meye P. Automatic detection and segmentation of brain metastases on multimodal MR images with a deep convolutional neural network. Comput Biol Med 2018;95:43–54.

[35] Ella Hassanien A, Moftah Hossam M, Taher Azar A, Shoman M. MRI breast cancer diagnosis hybrid approach using adaptive ant-based segmentation and multilayer perceptron neural networks classifier. Appl Soft Comput 2014;14:62–71.

[36] Ball CG, Butchart M, MacFarlane JK. Effect on biopsy technique of the breast imaging reporting and data system (BI-RADS) for non palpable mammographic abnormalities. Can J Surg 2002;45:259–63.

[37] Sathya PD, Kayalvizhi R. Optimum multi level image thresholding based on Tsallis entropy method with bacterial foraging algorithm. Int J Comput Sci 2010;7:336–43.

[38] Gonzalez RC, Woods RE. Digital image processing. 3rd ed. New Jersey: Prentice Hall, Incorpa.; 2009.

[39] Sumathi R, Arjunan S. Towards better segmentation of object of interest using histogram equalisation and morphological reconstruction. Int J Signal Imaging Syst Eng 2014;7:189–94.

[40] Jaccard P. The distribution of the flora in the alpine zone. New Phytol 1912;11:37–50.

[41] Huttenlocher DP, Klanderman GA, Rucklidge WJ. Comparing images using the Hausdorff distance. IEEE Trans Pattern Anal Mach Intell 1993;15:850–63.

[42] Jesorsky O, Kirchberg K, Frischholz R. Robust face detection using the Hausdorff distance audio and video-based biometric person authentication. 3rd International Conference AVBPA 2001 2001.

[43] Kaczynski K, Mikolajczak P. Information theory based medical image processing. OPTO-Electron Rev 2003;11:253–9.